



**Novel Gradient-diameter Magnetic Nanowire Arrays with
Unconventional Magnetic Anisotropy Behaviours**

Journal:	<i>ChemComm</i>
Manuscript ID	CC-COM-03-2018-002294.R1
Article Type:	Communication

SCHOLARONE™
Manuscripts



Journal Name

COMMUNICATION

Novel gradient-diameter magnetic nanowire arrays with unconventional magnetic anisotropy behaviors

Received 00th January 20xx,
Accepted 00th January 20xx

Jing Wang^a, Zhili Zuo^a, Liang Huang^a, Muhammad Asif Warsi^b, John Q. Xiao^{*b}, Jun Hu^{*a}

DOI: 10.1039/x0xx00000x

www.rsc.org/chemcomm

Fe-Co-Ni gradient-diameter magnetic nanowire arrays were fabricated by direct-current electrodeposition into a tapered anodic aluminium oxide template. In contrast to the magnetic behaviors of uniform-diameter nanowire arrays, it exhibited tailorable magnetic anisotropy that can be used to switch magnetic nanowire easily and unconventional temperature-dependent coercivity with much better thermal stability.

Modern recording media use magnetic granular films with perpendicular magnetization or magnetic anisotropy (PMA)^{1–4}, which are now facing so-called “tri-lemma” to further increase the storage density. To improve the signal-to-noise (SNR) ratio, one must use smaller grains to increase the number of grain within a magnetic bit cell. This leads to the reduction of thermal stability due to the superparamagnetic limit as thermal fluctuation at room temperature ($k_B T$) may overcome the energy barrier ($E=KV$) between two magnetization directions of an isolated grain with a volume V and an uniaxial anisotropy constant K . Without reducing the grain size, one can increase the thermal stability by increasing the value of K , which results in an unfavourable increase of coercivity, or an increase of difficulty of writing the bit. An innovative solution to solve this “tri-lemma” is to use a material with graded anisotropy^{5–7} where the coercivity is controlled by one end of material with low anisotropy and the thermal stability is controlled by the other end of material with high anisotropy. The graded anisotropy is so far achieved by changing material composition^{8, 9}. In this manuscript, we demonstrate an alternative method of using material shape to create graded anisotropy.

Magnetic nanowire arrays (MNWs) are an excellent choice to explore such a possibility. It is well known that the coercivity is inversely proportional to the nanowire diameter due to the combination of increased dipole interaction in nanowire array

with fixed nanowire separation (center-to-center distance) and reduced magnetization reversal via transverse wall modes which is difficult to move^{10–13}. At larger nanowire diameter, the dipolar interaction dominates the exchange coupling, leading to smaller coercivity. The magnetization reversal takes place via vortex wall mode in which the magnetization is no longer uniform at the position z along the wire axis^{14–16}. This “localized curling mode” is much faster than the transverse wall mode. Therefore a nanowire with gradient diameter that can host these two reversal modes can be imaged as a material with graded anisotropy. The coercivity at the thick end is small and can be reversed easily, while the thermal stability is controlled by the thin end of the wire.

Besides its potential as a material with graded anisotropy, nanowires with gradient diameter will impact other rich phenomena observed in magnetic nanowire array. For example, by changing the dipolar interaction, one can develop memory effect in magnetic nanowire array¹⁷, which can be used in analog recording media or sensors for detecting high intensity electromagnetic pulses. Magnetic nanowire array also shows tunable ferromagnetic resonance, which also closely related with dipolar interaction¹⁸. These properties will no doubt be modified by the nanowire with gradient diameter.

Inspired by this idea, we developed novel anodic alumina oxide (AAO) templates with gradient-diameter nanochannels using a two-step anodization. The templates were used to fabricate Fe-Co-Ni ternary alloy gradient-diameter magnetic nanowire arrays (defined as GDMNWs) by direct-current electrodeposition. The schematic illustration of the formation of GDMNWs is shown in **Fig. 1**. The magnetic properties of GDMNWs are compared with those of uniform-diameter magnetic nanowire arrays (defined as UDMNWs). UDMNWs show expected magnetic properties, i.e. the coercivity and anisotropy decrease with increasing nanowire diameter with

^a College of Chemical Engineering, Zhejiang University of Technology, Hangzhou 310014, China, E-mail: hjzjut@zjut.edu.cn.

^b Department of Physics and Astronomy, University of Delaware, Newark, DE 19716, USA, E-mail: jqx@udel.edu.

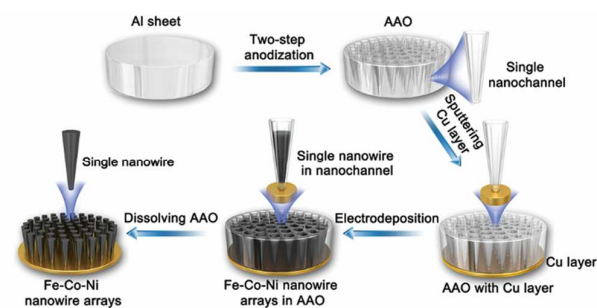


Fig. 1 Schematic illustration of the fabrication of GDMNWs.

fixed nanowire separation. Indeed GDMNWs shows magnetic properties expected from materials with graded anisotropy. The coercivity is low and is controlled by the thick end of nanowires, which leads to good writability. The extracted anisotropy is high, controlled by the thinner end of nanowires, indicating a good thermal stability. Surprisingly, the coercivity of GDMNWs increases with increasing temperature. This feature is rarely seen in common ferromagnets based on Fe, Co, and Ni. Such a property will be very useful for various applications.

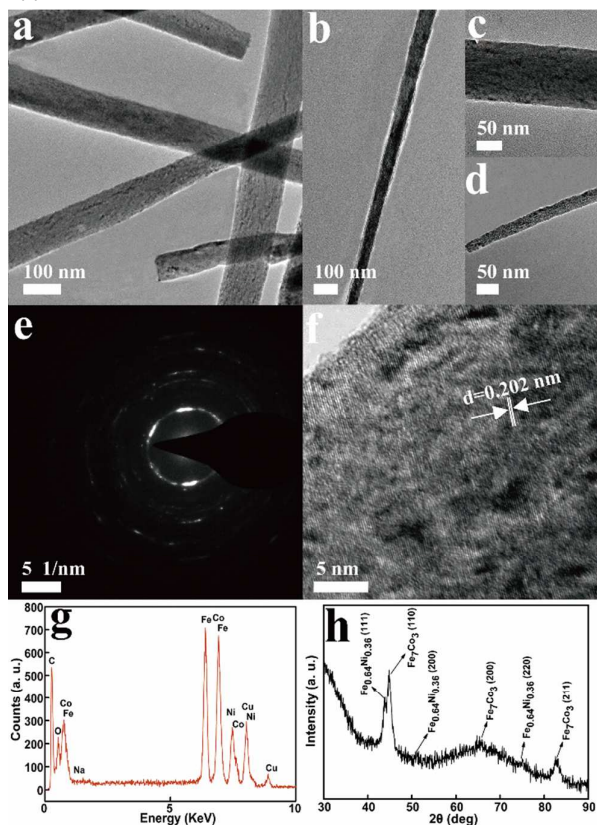


Fig. 2 TEM images of GDMNWs (a), single nanowire (b), thick end of single nanowire (c), and thin end of single nanowire (d). (e) SAED pattern of GDMNWs, (f) HRTEM image of a single nanowire, (g) EDS of a single nanowire, (h) XRD pattern of GDMNWs.

The SEM images of the top-view of AAO with gradient-diameter pores are shown in Fig. S1. The average diameter (d) and edge-to-edge separation (s) of the small pores at one side

of the template is about 27.7 ± 2.4 and 88.7 ± 7.3 nm, respectively, leading to the ratio of separation/diameter $s/d \approx 3.2$. The values of d and s for the large pores at other side are about 142.6 ± 5.3 and 33.4 ± 8.6 nm, respectively, with ratio of $s/d \approx 0.23$, respectively. The choice of these parameters is to ensure that exchange interaction within a nanowire dominates the dipolar interaction among nanowires at the thin end ($s > d$) and is opposite at the thick end ($s < d$). The pores density changes from $4.4 \times 10^4/\mu\text{m}^2$ to $10.6 \times 10^4/\mu\text{m}^2$, suggesting that about 2 smaller poles merging into a large pole. We estimated that the merged position occurs at the one-third of template thickness from the bottom (thin end) of the template. This fabrication method is very useful, offering a flexibility of making AAO with controlled gradient diameter. For comparison, we also prepared three corresponding templates with uniform diameters as shown in Fig. S2. The diameter, edge-to-edge distance and ratio of s/d were listed in Table S1.

The electrodeposition starts from the thin end and fills about $\frac{1}{4}$ of AAO thickness. The GDMNWs of $27.2 \mu\text{m}$ length were electrodeposited within AAO templates as shown in Fig. S3. A typical TEM image (Fig. 2a) of the GDMNWs detached from the AAO reveals that the prepared nanowires exhibit well-defined nanowire morphology and quite smooth surface. Fig. 2b confirms the single nanowire of GDMNWs has a roughly linear variation of diameter. Fig. 2c and Fig. 2d show typical thick and thin end of single GDMNW, respectively. The diameter and nanowire separation at the thick end are about 119 ± 1.2 nm and 33.4 ± 8.6 nm, resulting the ratio of s/d of about 0.28. The nanowire diameter and separation at the thin end are about 29.7 ± 1.4 nm and 88.7 ± 7.3 nm, giving rise to $s/d \approx 2.98$ that is closely resemble to that of bare AAO template. There are several strong and discontinuous rings with scattered spotty reflections from the select area electron diffraction (SAED) pattern of single nanowire as shown in Fig. 2e. The ring pattern indicates polycrystalline nature of GDMNW which is consistent with the results of XRD in Fig. 2h. The XRD pattern of the as-prepared GDMNWs can be indexed to bcc Fe_7Co_3 , and $\text{Fe}_{0.64}\text{Ni}_{0.36}$ with fcc structure. The lattice fringes can be clearly observed in the high-resolution TEM image displayed in Fig. 2f, revealing the crystallinity of the nanowire. The 0.202 nm periodicity of the fringes was compatible with the distance expected between the (110) planes of bcc Fe_7Co_3 phase. To further verify the composition of prepared nanowires, the components of GDMNWs were characterized by EDS as shown in Fig. 2g. The atomic ratio of Fe, Co and Ni element is about 10.13:10.11:4.13 (shown in Table S2). Fig. S4, Fig. S5 and Table S3 show the distribution of Fe/Co/Ni elements in the thick, middle, and thin segments of a single gradient-diameter nanowire. It is clear from Table S3 that the distribution of Fe, Co, and Ni along the nanowire axis is uniform. By changing the nanochannel diameters of AAO templates, the UDMNWs with diameter of 28.4 ± 1.4 (defined as UDMNWs-1), 77.3 ± 3.7 (defined as UDMNWs-2), and 122.3 ± 6.4 nm (defined as UDMNWs-3) were synthesized (Fig. S6). Furthermore, the values of the diameter, nanowire separation and the s/d in nanowire arrays with variously uniform diameter were listed in Table S4.

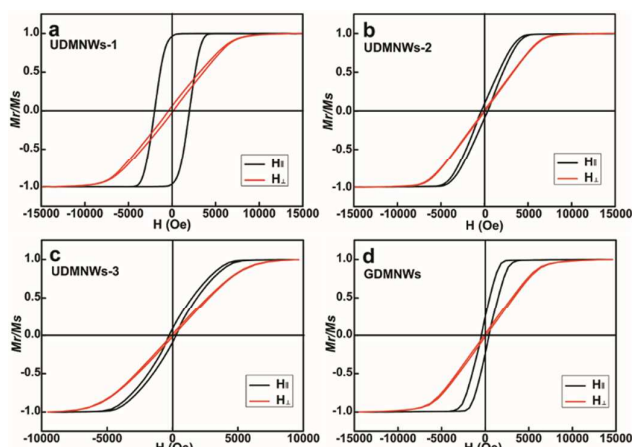


Fig. 3 Hysteresis loops measured with the external field applied parallel to nanowire axis ($H_{||}$) and perpendicular to nanowire axis (H_{\perp}) of the (a) UDMNWs-1, (b) UDMNWs-2, (c) UDMNWs-3, and (d) GDMNWs.

Fig. 3 reveals the magnetic hysteresis loops, measured by vibrating sample magnetometer, of Fe-Co-Ni ternary alloy MNWs with magnetic field applied parallel ($H_{||}$, black curve) and perpendicular (H_{\perp} , red curve) to the nanowire axis at room temperature. As shown in **Fig. 3** and listed in **Table S5**, the easy axes of all these samples are along the nanowire axis. For UDMNWs, the magnetic properties are very similar to reported results in literatures^{19–22}. For thin wires ($d_{\text{avg}}=28$ nm), the coercivity is high for the case of $H_{||}$ since the dipole interaction is small. In UDMNWs with $d_{\text{avg}} > 77$ nm, the coercivity is much reduced due to much enhanced dipolar interaction. This is also evident from much slanted hysteresis loops. Very interestingly, the coercivity of GDMNWs is similar to those of thick nanowires. This is desirable for good writability.

The thermal stability is determined by the effective magnetic anisotropy. We, therefore, calculate the effective magnetic anisotropy constant (K_{eff}) of the MNWs using the reported method²³:

$$K_{\text{eff}} = 2\pi M_s (H_{\perp}^5 - H_{||}^5)$$

where M_s is the saturation magnetization (emu/cm^3), H_{\perp}^5 and $H_{||}^5$ are the saturation magnetic fields perpendicular and parallel to the nanowire axis, respectively. It is all known that the saturation magnetization M_s varies with the nanowire diameters, here, we use a reported method (detailed description in Supporting Information) to calculate the M_s . The value of M_s for UDMNWs-1, UDMNWs-2, UDMNWs-3, and GDMNWs are approximately 1584, 953, 889, and 1237 emu/cm^3 , respectively. The K_{eff} of the prepared MNWs with different diameters is shown in **Fig. 4a**. Interestingly, the value of K_{eff} of GDMNWs is large and comparable to that of nanowire of the thinnest diameter. All the magnetic properties are summarized in **Table S5**. Indeed, the GDMNWs show similar behaviours to those materials of graded anisotropy, i.e. the coercivity is controlled by the magnetically soft end of nanowires and the thermal stability is controlled by the hard end. This can be understood that the reversal domain takes place at the thick end of the nanowire and the vortex wall

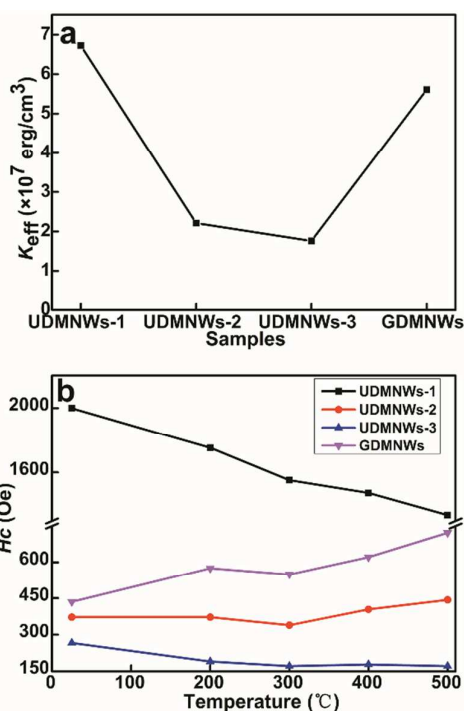


Fig. 4 (a) K_{eff} of each MNWs with different diameter, (b) coercivities at different measured temperature for each MNWs with different diameter.

propagates rapidly through the thick portion of the nanowire. This overwhelming magnetization reversal leads to low coercivity. To saturate the entire wire, the external magnetic field along with the dipolar interaction has to extend the domain wall into the thin portion of the nanowire, where the reversal takes place via traverse wall modes. Consequently, the effective K_{eff} is dominated by the thin portion of the nanowires. It should be mentioned that composition variation in nanowire array may also led to the change of magnetic anisotropy²⁴, which is not the case here due to rather uniform composition distribution in our samples (**Fig. S4**, **S5** and **Table S3**).

To further understand the thermal stability of the GDMNWs, demagnetization curves with $H_{||}$ were measured at different temperatures. As demonstrated in **Fig. 4b**, **Fig. S7**, **Fig. S8** and **Table S6**, the $H_{c||}$ of UDMNWs-1 decreased rapidly with increasing temperature. From the shape of the hysteresis loops (**Fig. S7a**), it seems that dipolar interaction is still weak and the reduction of the coercivity is due to the temperature dependence of the intrinsic anisotropy constant. For UDMNWs-2 the coercivity shows much weaker but increase slightly with temperature. For this sample, the ratio of s/d of about 0.98, suggesting that the dipolar interaction is already stronger than the exchange interaction. A much slanted hysteresis loop (**Fig. S7b**) also indicates much stronger dipolar interaction. The dipolar interaction will decrease the coercivity. The results seem to suggest that the dipolar interaction decreases with increasing temperature, resulting in a weak but increasing coercivity with temperature. For UDMNWs-3, the dipolar interaction is stronger, results in much smaller coercivity. At this low level of coercivity, the coercivity

very likely arises from structural defects and is insensitive to increase of temperature. Again, GDMNWs shows very interesting results with coercivity increase significantly with temperature as shown in Fig. 4b. This again may be explained with the reduction of dipolar interaction with temperature. The coercivity range is between 400 to 800 Oe where the coercivity is sensitively depending on the competition between the temperature dependence of the anisotropy and dipolar interaction. A small reduction of dipolar interaction can result in a large change of coercivity that overwhelms the temperature dependence of the anisotropy. The reduction of dipolar interaction may be due to the thermal agitation of the magnetization and domain wall structure, which is difficult to quantify. Nevertheless, such strong positive temperature coefficient in this common FeCoNi alloys have not been observed in other simple ferromagnets with bcc and fcc structure. The positive temperature coefficients have been observed in permanent magnet such as BiMn^{25–27}, and SmCoCuZrNb type of materials^{28–30}. The former is due to the phase transformation and the latter is due to the enhanced contrast of anisotropy between cell and cell boundary with temperatures. The positive temperature coefficients have also been observed in certain types of ferrite where two sublattices may have different temperature dependence. These mechanisms cannot be responsible for observed positive temperature coefficient of the coercivity in GDMNWs. Its origin is of scientific interests and it is certainly very useful for variety of applications.

In summary, GDMNWs have been successfully fabricated by direct-current electrodeposition method based on the AAO with the gradient-diameter nanochannels. The magnetic properties of GDMNWs are similar to those of gradient anisotropy, showing the coercivity and magnetic anisotropy are controlled by magnetically soft and hard ends, respectively. Very surprisingly, we observed very unusual and opposite temperature dependence of coercivity in GDMNWs as compared with those in UDMNWs. We speculate that such a temperature behaviour results from the competition of temperature dependence of dipolar and exchange interaction. Regardless the true mechanism, GDMNWs are very useful materials, offering the flexibility of tuning coercivity but with excellent thermal stability. Both properties are very useful in many applications ranging from recording media to microwave devices.

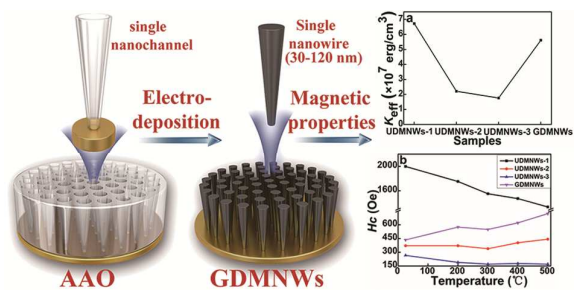
We gratefully acknowledge the financial support from National Natural Science Foundation of China (51672248 and 21405139) and Public Project of Zhejiang Province (2017C33172 and 2017C31049). The work done by John Xiao is supported by NSF DMR1505192.

Conflicts of interest

There are no conflicts to declare.

Notes and references

- 1 A. L. Ghoreyshi and R. H. Victora, *Appl. Phys. Lett.*, 2016, **108**, 1–4.
- 2 S. Kundu, N. Dwivedi, N. Satyanarayana, R. J. Yeo, J. Ahner, P. M. Jones and C. S. Bhatia, *ACS Appl Mater. Interfaces*, 2015, **7**, 158–165.
- 3 S. H. Liou and C. L. Chien, *Appl. Phys. Lett.*, 1988, **52**, 512–514.
- 4 Y. Kanai, *J. Appl. Phys.*, 1991, **69**, 4478–4480.
- 5 D. Suess, T. Schrefl, S. Fahler, M. Kirschner, G. Hrkac, F. Dorfbauer and J. Fidler, *Appl. Phys. Lett.*, 2005, **87**, 012504.
- 6 R. Skomski, T. A. George and D. J. Sellmyer, *J. Appl. Phys.*, 2008, **103**, 7F531–7F533.
- 7 Y. W. Jun, J. S. Choi and J. W. Cheon, *Chem. Commun.*, 2007, **0**, 1203–1214.
- 8 H. Yang, Y. Li, M. Zeng, W. Cao, W. E. Bailey and R. Yu, *Sci. Rep.*, 2016, **6**, 20427 1–9.
- 9 Z. Min, H. Z. Yang, J. Liu and R. H. Yu, *J. Appl. Phys.*, 2014, **115**, 17B514–17B514.
- 10 H. Forster, T. Schrefl, W. Scholz, D. Suess, V. Tsiantos and J. Fidler, *J. Magn. Magn. Mater.*, 2002, **249**, 181–186.
- 11 R. Hertel, *J. Magn. Magn. Mater.*, 2002, **249**, 251–256.
- 12 R. Hertel, and J. Kirschner, *Physica B*, 2004, **343**, 206–210.
- 13 H. Kronmüller and R. Hertel, *J. Magn. Magn. Mater.*, 2000, **215**, 11–17.
- 14 F. Vidal, Y. Zheng, P. Schio, F. J. Bonilla, M. Barturen, J. Milano, D. Demaille, E. Fonda and V. H. Etgens, *Phys. Rev. Lett.*, 2012, **109**, 1–5.
- 15 E. V. Vidal, Y. P. Ivanov, H. Mohammed and J. Kosel, *Appl. Phys. Lett.*, 2015, **106**, 1–4.
- 16 S. Choi, K. S. Lee, K. Y. Guslienko and S. K. Kim, *Phys. Rev. Lett.*, 2007, **98**, 087205.
- 17 X. M. Kou, X. Fan, R. K. Dumas, Q. Lu, Y. P. Zhang, H. Zhu, X. K. Zhang, K. Liu and Q. Xiao, *Adv. Mater.*, 2011, **23**, 1393–1397.
- 18 X. M. Kou, X. Fan, H. Zhu and J. Q. Xiao, *Appl. Phys. Lett.*, 2009, **94**, 112509.
- 19 X. H. Huang, G. H. Li, X. C. Dou and L. Li, *J. Appl. Phys.*, 2009, **105**, 084306–084310.
- 20 L. V. Thiem, L. T. Tu and M. H. Phan, *Sensors*, 2015, **15**, 5687–5696.
- 21 Y. W. Tan, L. R. Meng, Q. Peng and Y. D. Li, *Chem. Commun.*, 2011, **47**, 1172–1174.
- 22 M. Pousthomis, E. Anagnostopoulou, I. Panagiotopoulos, R. Boubekri, W. Q. Fang, K. A. Atmane, J. Y. Piquemal, L. M. Lacroix and G. Viau, *Nano Res.*, 2015, **8**, 2231–2241.
- 23 K. R. Pirota, E. L. Silva, D. Zanchet, D. Navas, M. Vazquez, M. Hernandez-Velez and M. Knobel, *Phys. Rev. B*, 2007, **76**, 233410.
- 24 V. Vega, T. Bohnert, S. Martens, M. Waleczek, J. M. Montero-Moreno, D. Gorlitz, V. M. Prida and K. Nielsch, *Nanotechnology*, 2012, **23**, 465709.
- 25 D. T. Zhang, S. Cao, M. Yue, W. Q. Liu, J. X. Zhang and Y. Qiang, *J. Appl. Phys.*, 2011, **109**, 07A722 1–3.
- 26 Y. C. Chen, G. I. Gregori, A. Leineweber, F. Quc, C. C. Chen, T. Tietze, H. Kronmüller, G. Schütz and E. Goering, *Scripta Mater.*, 2015, **107**, 131–135.
- 27 K. Koyama, Y. Mitsui and K. Watanabe, *Sci. Technol. Adv. Mater.*, 2008, **9**, 024204–024208.
- 28 T. Chen and W. Stutius, *IEEE Trans. Magn.*, 1974, **10**, 581–586.
- 29 X. Guo, X. Chen, Z. Altounian and J. O. Strom-Olsen, *J. Appl. Phys.*, 1993, **73**, 6275–6277.
- 30 P. Gaunt, *Phil. Mag. B*, 1983, **48**, 261–276.



Gradient-diameter magnetic nanowires exhibited tailorable magnetic anisotropy that can be used to switch magnetic nanowire easily and unconventional temperature-dependent coercivity